Aircraft Model Aerodynamic Forces and Longitudinal Stability

Gayathri Kola
The University of Texas at Arlington, Arlington, Texas, 76019, United States

This experiment investigates the forces acting on a 1:50 scale Model A-7 Corsair using an AFA3 three-component force balance. The model undergoes angle of attack sweeps from 0° to 20° in 2° increments while mounted upside-down and rotated manually. The resulting coefficients of lift and drag, as well as the pitching moment, exhibit unexpectedly high values and scattered data points. Electrical influences on voltage readings from load cells may contribute to these discrepancies. The experiment's Reynolds number is 340,340.23, lower than the laminar flow threshold for a flat plate of 500,000, suggesting dominant viscous forces due to the model's complex geometry. Comparisons with the full-scale model's Reynolds number of 17,902,827 highlight the importance of various parameters velocity, viscosity, and density that affect the Reynolds number. Precautions, including automated angle changes and avoiding high freestream dynamic pressure ranges of the wind tunnel operation, are recommended to minimize errors. Prolonged wind tunnel operation should be avoided to prevent temperature-induced effects. Additionally, variations in the pitching moment coefficient against the angle of attack show no clear trend, possibly due to electrical disturbances in voltage measurements, emphasizing the need for further investigation.

I. Nomenclature

$Fore$	=	force of fore load cell
Aft	=	force of aft load cell
$Drag$	=	drag force from the drag load cell
F	=	force
K	=	slope
V	=	measured voltage
V_{offset}	=	voltage at no force applied
B	=	y-intercept
g	=	acceleration due to gravity, 9.81 m/s^2
$C_{m,cg}$	=	pitching moment about the center of gravity
d_v	=	vertical distance from model centerline to model CG.
d_h	=	horizontal distance from model CG to mounting sting arm CG.

II. Introduction

Wind tunnel experiments are important for characterizing the forces and moments experienced by a given aircraft geometry from a small-scale model. These characteristics all one to predict the performance of the aircraft, if the design is sufficient or if it must modified for better lift, reduced drag, or other aerodynamic trade-offs. Their smaller size and ability to test models with conditions of flow uniformity and low turbulence means they can replicate as close to ideal conditions as possible. It is less expensive than full-scale model testing and can give decent estimates. The acceleration due to gravity is assumed to be 9.81 m/s^2 for this experiment, although more precise methods can be used based on location [1]. Previously, an AFA3 three-component force balance was calibrated using increasing loads to ensure that the instrument was producing reliable data.

In this experiment, the same AFA3 force balance is used to measure the forces and moments acting on a 1:50 scale model of Vought A-7 Corsair aircraft. The force balance is connected with three load cells that measure

fore, aft, and drag forces. The load cells work by recording the voltage produced from small displacements of strain gage within. The load cells have a Wheatstone bridge arrangement where the change in resistance due to the addition of some force causes a voltage difference at the sensing element. The model is mounted on a sting arm of a given length. Due to the setup, the model and mounting arm may add to deflections due to existing U-joints. The placement of these joints added to translational and rotational motion – which are acceptable for a small specified range. Large levels of deflection can cause data inaccuracies. This can affect the force and moment data [1].

The mounted model is swept through the angles of attack from 0° to 20° in 2° increments. Since the force balance must be in tension to measure a voltage in the load cell, the model is moved down in an anticlockwise direction. There are two mounting positions – normal to the flow direction and mounting with a sting arm rearward of the model. Mounting the model normally to the flow can introduce structural distances, thus, it is placed rearward of the model. Also, allows for the freestream flow to move smoothly along the surface of the model whilst the normal mounting position would create flow interferences on the lower surface of the model [1].

The following Eq. (1-3) are used to determine the lift, drag, and pitching moment of the mounting sting arm from the results obtained via the force balance [1].

$$Lift\ (N) = Fore\ (N) + Aft\ (N) \tag{1}$$

$$Drag\ (N) = Drag\ (N) \tag{2}$$

$$Pitching\ Moment\ (Nm) = \big(Fore\ (N) - Aft\ (N)\big) * 0.0635 \tag{3}$$

III.Experimental Procedure

A. Apparatus

In this experiment, an AFA3 three-component force balance is used as seen in Fig. 1. It consists of a mounting plate, a force plate, and a model mounting point. It is connected to the AF100 subsonic wind tunnel via the mounting plate. It utilizes three load cells that measure fore and aft lift forces and drag forces. A Vought A-7 Corsair aircraft model is connected to a sting mount arm for this test. The wind tunnel model and the force balance used are from TecQuipment Ltd. The sting mount arm is custom-made along with the Pitot tube connected using a Velmex Inc QC110-AR stepper controller [1].

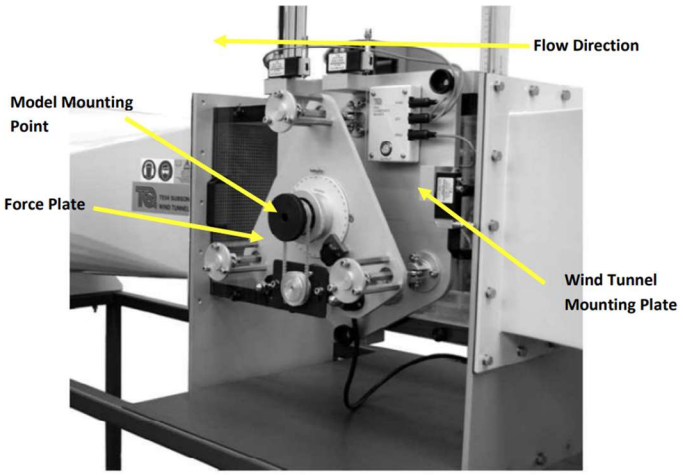

Fig. 1 AFA3 force balance connected to AF100 wind tunnel [1].

The A-7 Corsair model connected to the sting mount arm is shown in Fig. 2. Two positions are shown, the first on the left is the model at 0° of angle attack and on the right at 20°. The Pitot tube measures the freestream dynamic pressure and this reading is indicated on the manometer located on the front white panel of the wind tunnel. The model mounting point is used to change the angle of attack from 0° to 20° in 2° increments. The data is collected by a Dell PC with an external data acquisition system (PCI-6034E DAQ card) and an SCB-68 DAQ connection box.

The computer hosts LabView software that displays the data collection interface as seen in Fig. 3 [1]. Note, that the model is placed upside down and the angle of attack is negative. This is done since the force balance has to be in tension to measure the voltage.

Fig. 2 Positions of A-7 Corsair model, initial (left) and final (right) [1].

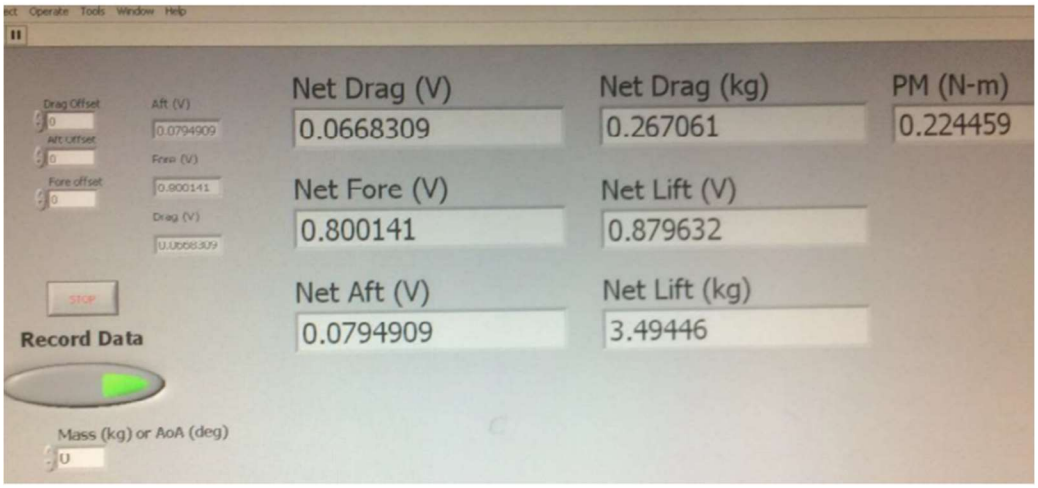

Fig. 3 LabView interface on the computer unit [1].

B. Procedure

For safety, the operation of the force balance must have a dynamic pressure below 20 mm of Hg. The freestream velocity of the wind tunnel must also be low because the mount sting arm can produce a large moment. To start the experiment, the Power Display Module from the wind tunnel is switched on and allowed to warm up for about 15 minutes as per the manufacturer's recommendation [1].

Meanwhile, the room temperature and pressure are recorded from the thermometer and barometer connected to a wall in the room. The recorded temperature and pressure for this experiment are **20**℃ and **744.9 mm of Hg**.

The A-7 model is mounted onto the sting arm and connected to the AFA3 force balance using the mount collar. The model and the sting must be positioned horizontally in the flow direction. The goniometric wheel is used to set the angle of attack to 0°. Once positioned correctly, the setup is locked in place by tightening the lock collar. Then, the LabView software is switched on. The values for the force balance showing fore, aft, and drag voltages are not zero since the model is mounted. Instead, the offset readings are recorded at 0° angle of attack and stored in one separate data file. The dynamic pressure is measured to be **20 mm of H_2O**. The readings for each angle attack are taken for approximately 5 seconds. This is repeated for 0° to 20° angle of attacks while manually changing it using the goniometric wheel [1].

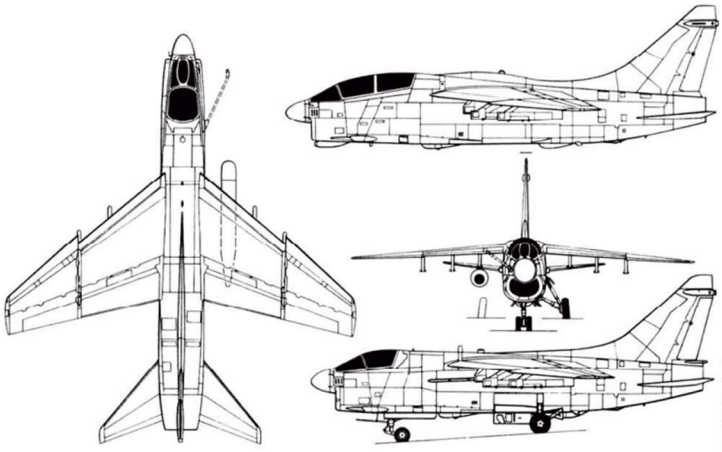

Fig. 4 Three-view drawing of A-7 Corsair aircraft [1].

The Fig. 4 is the three-view drawing of the A-7 aircraft. Fig. 5 gives the locations of CG for the model, the entire system, and the mount sting arm as well as their distances and the mean aerodynamic chord (MAC). This Fig. 5 will be used for moment calculations discussed in Section IV including data reduction. In total, there are two separate files obtained – offset data and actual voltage measurements from the angle attack range of 0° to 20° [1].

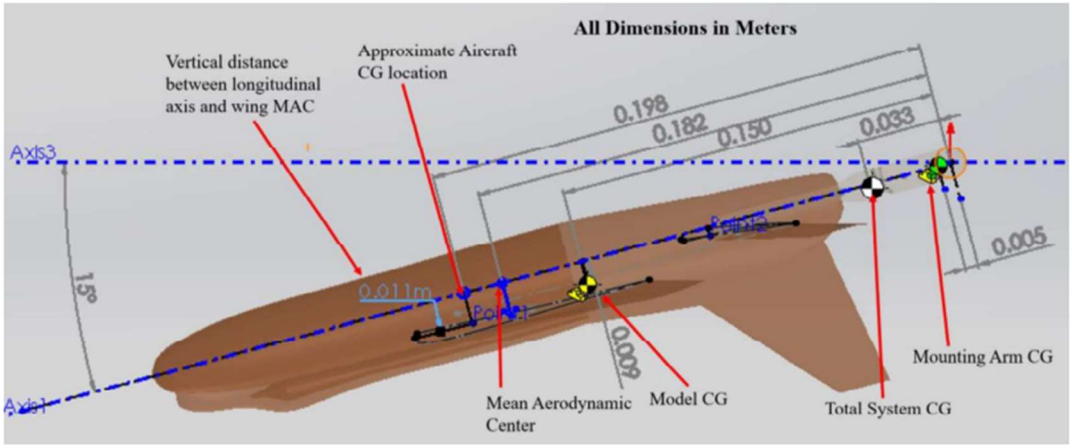

Fig. 5 Locations of CG for the system and model CG of the aircraft [1].

IV. Results and Discussion

For the data processing part, the freestream dynamic pressure from the wind tunnel manometer is converted to SI units using the conversion factor: 1 mm of H2O = 9.8065 Pa. The room temperature and pressure are converted to SI units using 0℃ = 273.15 K and 1 mm of Hg = 133.3224 Pa. Using the conversions, the room temperature and pressure are 293.15 K and 99,311.86 Pa. The freestream dynamic pressure is 196.13 Pa. Assuming a gas constant, R with a value of 287 J/(kg-K) for air, the density of air is calculated using the ideal gas law given in Eq. (4):

$$\rho_\infty = \frac{P_\infty}{RT_\infty} \tag{4}$$

The freestream density obtained is 1.18 kg/m^3. Using the freestream density and known freestream dynamic pressure the freestream velocity is calculated using:

$$U_\infty = \sqrt{\frac{2q_\infty}{\rho_\infty}} \tag{5}$$

The freestream velocity obtained is 18.23 m/s. Then, the average values of fore, aft, and drag data are found for the offset data file. In total, there must be three values for fore, aft, and drag voltages at 0° angle of attack. Once offset averages are obtained, the averages for each angle of attack (from 0° to 20°) are calculated using the second data file.

Using the offset averages and actual data averages, the corrected voltage is found using:

$$V_{corrected} = \left(V - V_{offset}\right) \tag{6}$$

Where V is the voltage average from the actual data set from 0° to 20° and V_{offset} is from the offset averages. Then, the raw forces for the fore, aft, and drag load cells are found using the respective calibration curve given in Fig. 6-7. The calibration curve is given in the form of:

$$F = K * \left(V - V_{offset}\right) + B \tag{7}$$

Where K is the slope of the curve, B is the y-intercept and F is the corresponding force in newtons (N).

The geometric dimensions of the model aircraft are given in Table 1 below and Fig. 5.

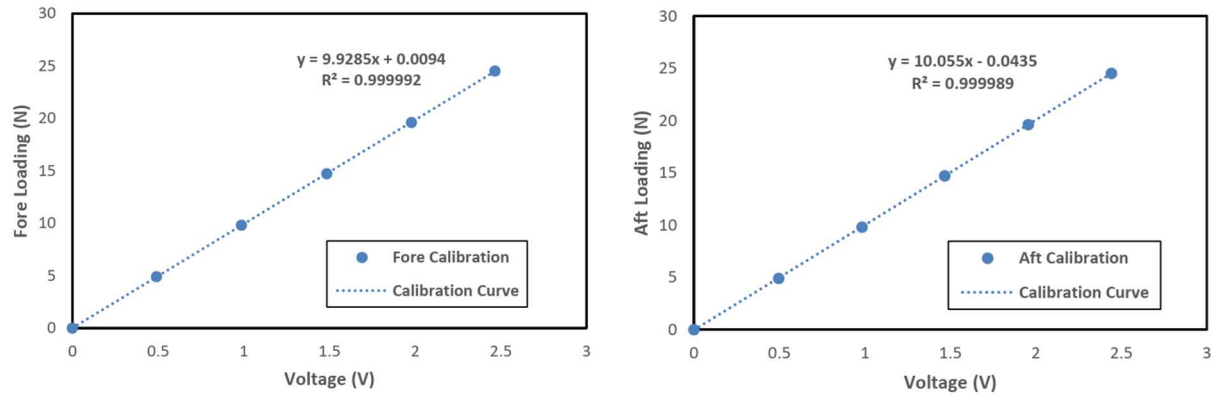

Fig. 6 Calibration curve for fore (left) and aft (right) load cell [2].

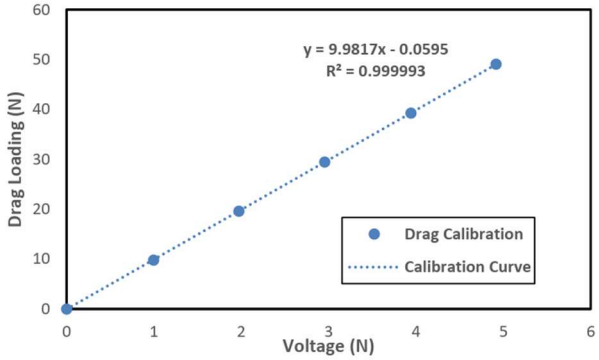

Fig. 7 Calibration curve for drag load cell [2].

Table 1. Geometric dimensions of the mounted aircraft model [1].

Description	Value	Units
Model scale	1:50	-
Model length	0.287	m
Wing span	0.236	m
Wing area	0.01393	m^2
Mean aerodynamic chord	0.0661	m
Distance from rotational axis to total system CG	0.33	m
Distance from the rotation axis to the nose	0.367	m
Distance from the tail of the aircraft to the rotational axis	0.045	m
Distance from rotational axis to wing MAC	0.182	m
Distance from rotational axis to original aircraft CG	0.199	m
Model mounting arm mass	0.31	kg
Model mass	0.15	kg

Table 2 presents the results for the forces obtained for fore, aft, and drag load cells using corrected voltages.

Table 2. Corrected results from fore, aft and drag load cells.

AOA [deg]	Fore [N]	Aft [N]	Drag [N-m]
0	0.298396	-0.248947	0.334060
2	2.640681	-0.103991	1.320627
4	7.760469	6.572089	0.023754
6	6.948162	4.542422	2.008315
8	8.896454	6.114642	0.733898
10	9.669254	4.508022	1.130194
12	9.056078	1.868351	0.981415
14	9.230686	2.222706	0.783665
16	9.699318	3.357240	2.598130
18	11.813805	4.615300	-0.063924
20	7.881482	-2.361968	2.136732

Once, the forces are obtained, the total forces lift and drag, and pitching moment can be calculated using Eq. (1-3). The results are presented below in Table 3. The corresponding lift and drag coefficients are calculated using Eq. (8-9).

$$C_L = \frac{L}{q_\infty S_{ref}} \tag{8}$$

$$C_D = \frac{D}{q_\infty S_{ref}} \tag{9}$$

From above, S_{ref} is the wing reference area obtained from Table 1 with a value of 0.01393 m^2. The following results are visualized by plotting lift and drag coefficients against the angle of attack in Fig. 8-10. Notice, that the values of lift and drag coefficients are higher than expected. This irregularity is seen in the plots as well since there is no clear trend observed from the data. This could potentially be due to electrical disturbances that may have interfered with data collection.

Table 3. Results of lift, drag, and pitching moments along with coefficients.

AOA [deg]	Lift [N]	Drag [N]	Pitching Moment [N-m]	C_L [-]	C_D [-]
0	0.049449	0.334060	0.034756	0.018099	0.122273

2	2.536690	1.320627	0.174287	0.928479	0.483376
4	14.332558	0.023754	0.075462	5.246003	0.008694
6	11.490583	2.008315	0.152764	4.205784	0.735083
8	15.011096	0.733898	0.176645	5.494362	0.268621
10	14.177276	1.130194	0.327738	5.189167	0.413674
12	10.924429	0.981415	0.456421	3.998560	0.359218
14	11.453392	0.783665	0.445007	4.192171	0.286837
16	13.056558	2.598130	0.402722	4.778962	0.950968
18	16.429104	-0.063924	0.457105	6.013381	-0.023398
20	5.519514	2.136732	0.650459	2.020253	0.782087

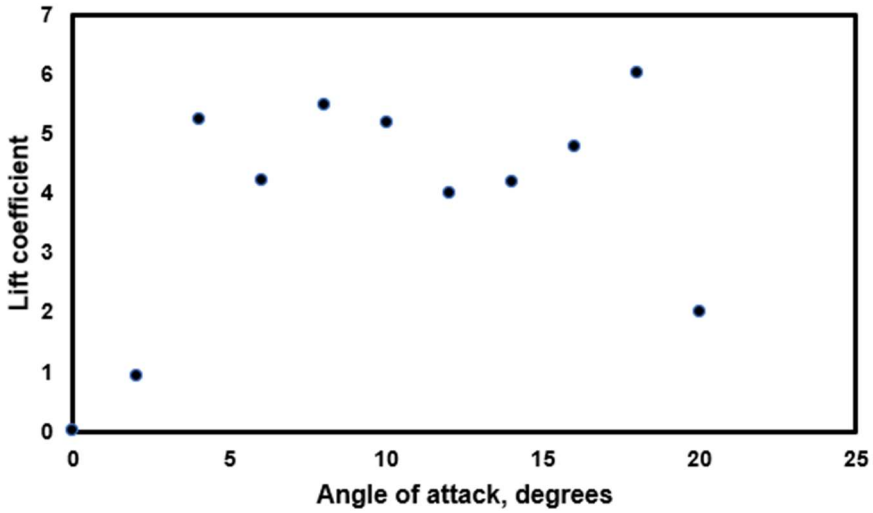

Fig. 8 Lift coefficient versus angle of attack.

There is no followed trend in the lift-curve-slope. Hence, the maximum lift coefficient observed may be incorrect.

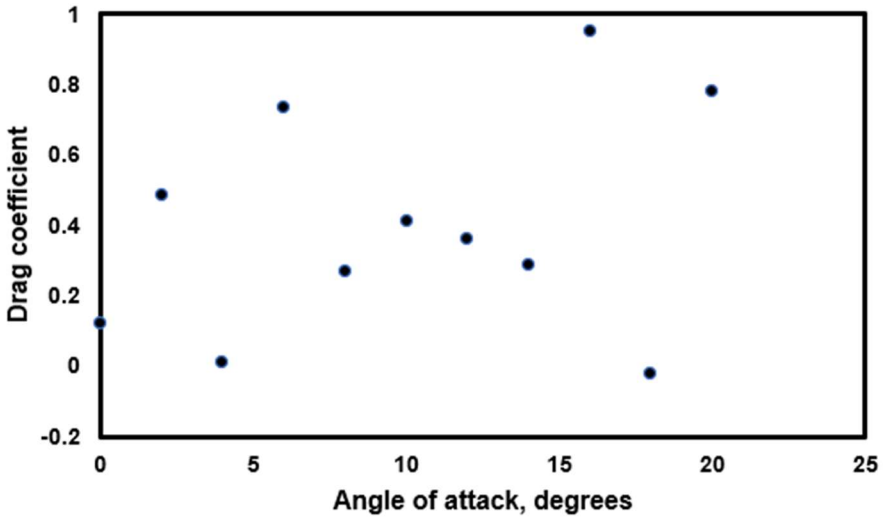

Fig. 9 Drag coefficient versus angle of attack.

Again, there is no trend for the drag data either, all data points are scattered. Thus, this data set may not be usable.

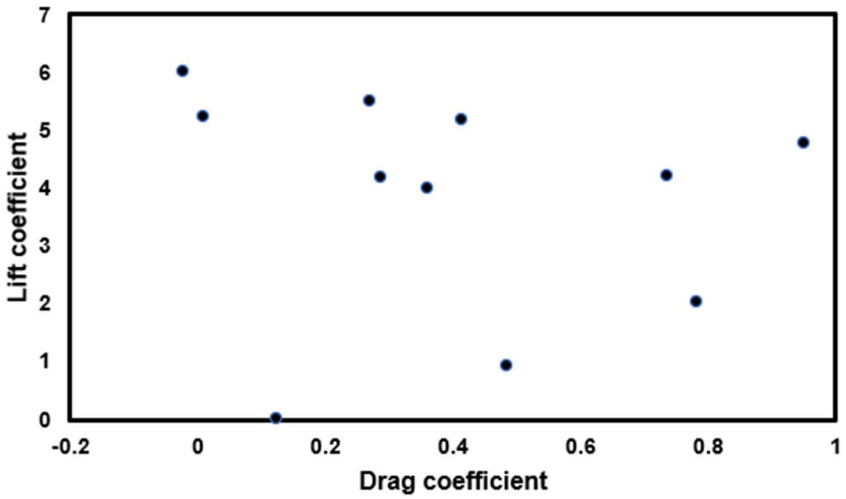

Fig. 10 Drag polar.

Lastly, the drag polar is plotted. Due to the scattered nature of the plot, the zero-lift drag coefficient cannot be determined since there is no expected trendline (a 'C' curve). There may be issues with the load cell readings, specifically fore and aft load cells. However, the electrical influences may have disturbed readings from all three load cells.

Lastly, a Reynold number comparison is performed for the experiment and the actual aircraft length as the reference dimension. The Reynolds number is the ratio of inertial forces to the viscous forces of a fluid. It is a function of several parameters, including density, dynamic viscosity, velocity, and characteristic length. A higher Reynolds number typically indicates higher turbulence levels and lower viscosity, and vice-versa. Wind tunnel experiments are conducted to understand the flow characteristics of a given aircraft geometry or airfoil. By knowing the Reynolds number, the type of flow can be anticipated – where it will it laminar or turbulent. This allows us to calculate the expected lift and drag coefficients which will be useful for predicting the forces experienced by the full-scale model. To obtain the viscosity of air, the Sutherland's law is used:

$$\frac{\mu}{\mu_0} = \left(\frac{T}{T_0}\right)^{\frac{3}{2}} \left(\frac{T_0 + S_\mu}{T + S_\mu}\right) \tag{10}$$

The value of $\mu_0 = 1.716 \cdot 10^{-5}$ (N-s)/m^2, $T_0 = 273$ K, $S_\mu = 111$ K are obtained for air [3]. The viscosity calculated is $\mu = 1.814 \cdot 10^{-5}$ (N-s)/m^2. Using the calculated value for viscosity, The Reynolds number can be calculated from Eq. (11):

$$Re_{exp} = \frac{\rho U_\infty L}{\mu_\infty} = \frac{(1.18)(18.23)(0.287)}{1.814 \cdot 10^{-5}} = 340{,}340.23 \tag{11}$$

Hence, the Reynolds number for this experiment, $Re = 3.4 \cdot 10^5$. Now, we will assume the standard day conditions of air temperature at 15℃ or 288.15 K, pressure at 1 atm or 101,325 Pa, and density at 1.225 kg/m^3. These numbers are used to calculate the Reynolds number of the full-scale aircraft. Using the scale ratio of 1:50 and model length of 0.287 m, the total aircraft length is calculated to be 14.35 m. Then, using the Sutherland's law, the viscosity of air is estimated to be $1.79 \cdot 10^{-5}$ (N-s)/m^2. The aircraft has the largest angle of attack ranges during takeoff and landing phases, using the same velocity of the experiment, the Reynolds number is calculated:

$$Re_{flight} = \frac{\rho U_\infty L}{\mu_\infty} = \frac{(1.225)(18.23)(14.35)}{1.79 \cdot 10^{-5}} = 17{,}902{,}827.5 \tag{12}$$

The flight Reynolds number is $Re = 1.79 \cdot 10^7$, much higher than the experimental value. It is anticipated to have an even higher value since in real conditions, the actual speed of the aircraft during takeoff and landing is typically higher than 18.23 m/s. A higher Reynold's number indicates a faster transition to turbulence, which is the case for the full-scale model when compared with the experiment.

For this experiment, the potential sources of error come from electrical influences that contributed to scattered data that show no trend as seen in Fig. 8-10. Apart from this, errors may come from the manual change in angle of attack when the goniometric wheel was used. Whenever it is changed, the model is observed to shake slightly which could disrupt the airflow. Hence, to mitigate possible errors the shaking, one can wait for a few seconds before the data is recorded for each angle of attack. However, running the wind tunnel for too long can increase heat and produce temperature effects. Instead, an automatic system can be placed that changes the angle attack precisely and with the same rate of turn. Errors may emerge from not aligning the model correctly to the respective angle of attack. Another source of error could be from operating at 20 mm of Hg freestream dynamic pressure – we have performed this experiment under safety conditions. In the future, this experiment could be performed at a lower freestream dynamic pressure. Given the geometry of the model and the short length of the sting arm, the flow may interfere with force measurements. Placing the model at a larger distance away from the mounting point may produce less interference. Lastly, another source of error is while recording the data for approximately 5 seconds each time – a timer can be used that automatically records and stops.

During calibration, the voltages measured from the fore and aft load cells were positive because the loads were equally distributed. With the mounting method, the aft load cell gave some negative readings of voltage. This may be acceptable since the voltage range during calibration was $\pm$ 10 V. So, it is capable of measuring negative voltages. The negative voltage readings may be present since a mounting sting arm is used, and the model is placed a certain distance away from the mounting point which may already create a small moment.

The offset provided at 0° should be sufficient, however, it can be provided for each angle of attack. Although this could improve the data, the wind tunnel should not be operated for long periods. As mentioned, long run-time may develop an increase in temperature which may influence freestream flow characteristics. So, if an offset data file is collected for each angle of attack, it would mean longer operation and multiple files.

(EXTRA CREDIT)

The pitching moment of the aircraft model can be calculated by first splitting the components of the distances from CG of the sting mount and model using Eq. (13-14). The distance from the mounting arm CG and model CG is 0.15 m from Fig. 5. The vertical distance from the model centerline and model CG line is 0.009 m. However, this distance changes as the angle of attack is increased such that:

$$d_v = (\sin\alpha \cdot 0.15) + 0.009 \tag{13}$$

$$d_h = (\cos\alpha \cdot 0.15) \tag{14}$$

Where, d_v is the vertical distance from the model centerline and model CG line as a function of the angle of attack α. The d_h is the horizontal component of distance from model CG to mounting sting arm CG. Then, the moment about model CG is calculated by:

$$M_{cg} = -(L \cdot d_h) - (D \cdot d_v) + M_{raw} \tag{15}$$

Where, M_{raw} is the raw pitching moment calculated and presented in Table 3. It is the moment calculated from the sting mounting arm. Then, the pitching moment coefficient can be calculated using Eq. (16). The $\bar{c}$ is the mean aerodynamic chord of the wing with a value of 0.0661m.

$$C_{m,cg} = \frac{M_{cg}}{q_\infty S_{ref} \bar{c}} \tag{16}$$

The results obtained from the procedure above are given in Table 4 and plotted in Fig. 11.

Table 4. Results from the moment about the center of gravity.

AOA [deg]	M_{cg} [N-m]	$C_{m,cg}$ [-]
0	0.024332	0.134738
2	-0.224784	-1.244712
4	-2.069647	-11.460397
6	-1.610945	-8.920394
8	-2.075032	-11.490217
10	-1.806156	-10.001349
12	-1.185875	-6.566626
14	-1.257461	-6.963023
16	-1.610698	-8.919027
18	-1.883108	-10.427460
20	-0.256389	-1.419722

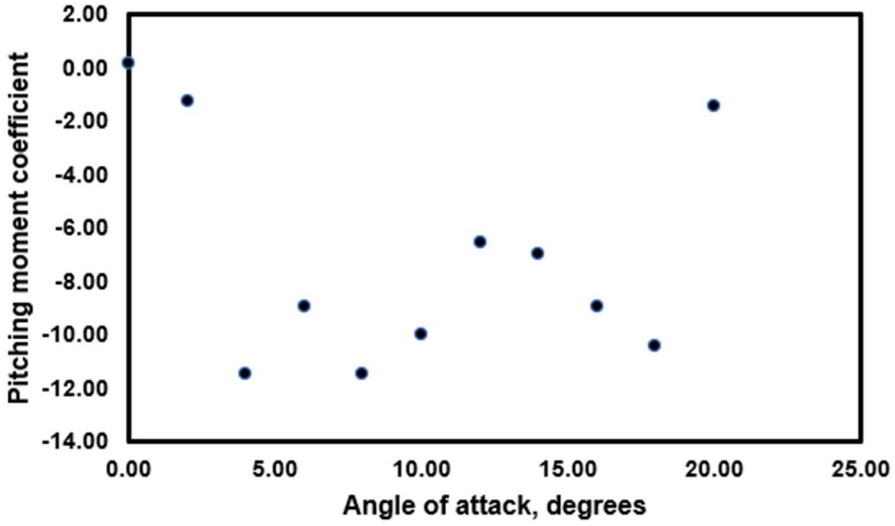

Fig. 11 Pitching moment coefficient versus angle of attack.

Since, the data and results obtained do not show a reliable trend, pitching moment plots are also inconclusive. Also, the values of the pitching moment coefficient about the center of gravity are very high, which is not expected.

V. Conclusion

In this experiment, the forces acting on a 1:50 scale Model A-7 Corsair are determined using an AFA3 three-component force balance. The model is mounted using a sting arm from the back, creating a small distance from model CG to mounting arm CG. The fore, aft, and drag load cells measure the voltage when the model experiences an amount of force. The model is mounted upside-down and rotated counter-clockwise from the horizontal axis to keep tension for the force balance. It is swept from an angle attack range of 0° to 20° in 2° increments and rotated manually via a goniometric wheel. The lift, drag, and pitching moments are calculated from the forces obtained from calibration curves.

Upon processing the data, it was evident that the coefficients of lift and drag were significantly high compared to typically expected values. The lift-curve-slope and drag versus angle of attacks plots show scattered data points with no clear trend seen – usually, there is a linear region for the lift-curve-slope with a stall point. Similarly, the drag polar also did not give any visible trend, following a scattered, patternless plot. The vast variation in results can be traced back to voltage readings from the fore, aft, and drag load cells. There may have been electrical influences that have contributed to disturbed readings.

The experiment's Reynolds number was calculated to be 340,340.23, which is below 500,000 for the laminar flow of a flat plate. The viscous forces can be dominant due to the complex geometry of the aircraft model. It is compared with the full-scale model Reynolds number of 17,902,827. The higher value of the Reynolds number can be related to the fact that this quantity is dependent upon many parameters and increasing the length yielded in a

higher Reynolds number. The velocity was kept constant for this comparison, however, actual flight conditions such as takeoff or landing would result in a higher Reynolds number. Standard conditions were used to calculate the flight Reynolds number.

To minimize errors in the experiment, precautions include avoiding manual changes in the angle of attack to prevent model shaking and airflow disruption. Waiting a few seconds before recording data for each angle helps mitigate these issues. An automatic system for precise and consistent angle changes is recommended. Misalignment of the model and operating at high freestream dynamic pressure can introduce errors; adjusting the model's distance from the mounting point and conducting experiments at lower pressure may help. During calibration, negative voltage readings from the aft load cell are acceptable due to the mounting method. While providing offsets for each angle of attack could enhance data, prolonged wind tunnel operation should be avoided to prevent temperature-induced effects on freestream flow characteristics.

Lastly, the pitching moment about the center of gravity of the model was calculated for the range of angle of attacks. Using the pitching moment results, the coefficient of pitching moment was plotted against the angle of attack. As expected, there was no noticeable trend seen due to the potential electrical disturbances in voltage measurements. Due to the unclear trends in the data, the experiment must be repeated while accounting for the discussed sources of errors.

References

[1] "MAE 3182 | Aircraft Model Aerodynamic Forces and Longitudinal Stability.," The University of Texas at Arlington, MAE Department, Spring 2022.

[2] "MAE 3182 | Experiment 5 Calibration Curves," The University of Texas at Arlington, MAE Department, Fall 2023.

[3] "Sutherland's Law." Retrieved 31 October 2023. https://doc.comsol.com/5.5/doc/com.comsol.help.cfd/cfd_ug_fluidflow_high_mach.08.27.html